Polarizabilities of Rn-like Th^{4+} from rf spectroscopy of Th^{3+} Rydberg levels

Julie A. Keele and S. R. Lundeen[*]

Department of Physics, Colorado State University, Fort Collins, Colorado 80523, USA

C. W. Fehrenbach

J.R. Macdonald Laboratory, Kansas State University, Manhattan, Kansas 66506, USA

High-resolution studies of the fine-structure pattern in high-L $n = 37$ levels of Th^{3+} have been carried out using radio-frequency (rf) spectroscopy detected with resonant excitation Stark ionization spectroscopy (RESIS). Intervals separating $L = 9$ to $L = 15$ levels have been measured, and the results analyzed with the long-range effective potential model. The dipole polarizability of Th^{4+}is determined to be $\alpha_D = 7.720(7)$ a.u. The quadrupole polarizability is found to be 21.5(3.9) a.u. Both measurements represent significant tests of *a priori* theoretical descriptions of this highly relativistic ion.

PACS number(s): 32.30.Bv, 32.10.Dk, 32.10.Fn

I. INTRODUCTION

The radonlike Th^{4+} ion is the most common charge state of thorium in chemical compounds. Understanding the chemistry of thorium and other actinide elements is important to many national priorities, but very little experimental data exist to check the *a priori* theoretical methods used to describe the ions that are at the heart of that chemistry. For example, no optical spectroscopy of excited levels of Th^{4+} has been reported. The most significant dynamic characteristics of the $^1S_0$ ground state of Th^{4+} are its dipole and quadrupole polarizabilities. They control important aspects of the long-range interactions of the Th^{4+} ion with ligands or electrons. These properties can be measured by studying the binding energies of high-L Rydberg levels of Th^{3+}, bound to the Th^{4+} ground state. A recent study of this type using the RESIS technique reported the first measurements of the dipole and quadrupole polarizabilities of Th^{4+} [1]. The reported precision was $\sim$1% and $\sim$20%, respectively. In order to obtain better measurements, we report here a study in which rf spectroscopy was used to directly measure intervals separating $n = 37$ levels of Th^{3+} with $9 \leqslant L \leqslant 15$. This builds on the previous study as the RESIS method was used to detect the population change in particular high-L $n = 37$ levels caused by an rf-induced transition. The resulting measurement improves the precision of the dipole polarizability by an order of magnitude, but indicates that the previous report of the quadrupole polarizability was an overestimate.

II. EXPERIMENT

The technique used for this study is similar in principle to that used for a previous study of high-L Rydberg states in Si^{2+} [2]. The apparatus used here is a slightly modified version of that used for two recent optical RESIS studies [1,3] and is illustrated schematically in Fig. 1. A beam of 100 keV Th^{4+} ions is extracted from an electron cyclotron resonance (ECR) ion source, mass selected, and focused through a dense Rb Rydberg target. A significant fraction (3%–6%) of the Th^{4+} ions capture a single electron from the target Rb atoms to form highly excited Rydberg levels of Th^{3+}. After charge capture, the Th^{3+} beam is magnetically selected and focused by the strong electric field in an electrostatic lens, which also has the effect of Stark ionizing the very weakly bound Th^{3+} levels that will later form the upper state of the RESIS excitation.

The Rydberg target was excited to the 10F level, so it is expected that the most populated Th^{3+} levels have binding energies of $\sim$0.3 $\pm$ 0.1 eV, i.e., they are near $n = 30$ [4]. Several possible RESIS transitions upwards from these levels were observed in the optical RESIS study [1]. One of them, the $n = 37$ to $n' = 73$ transition using the 10P(10) CO$_2$ laser line, was used for this study. As illustrated in Fig. 1, two CO$_2$ laser interaction regions were used here, separated by a region where an rf electric field could be applied. In both laser regions, the angle of intersection with the Th^{3+} beam was adjusted to Doppler-tune the CO$_2$ laser into resonance with the excitation of one particular $n = 37$ level. As an example, consider observation of the $L = 11$ to $L = 12$ transition, where both laser regions are tuned to excite the $n = 37$, $L = 11$ to $n = 73$, $L = 12$ transition. In this case, the first region depletes the population of the $L = 11$ level, insuring a population difference with the neighboring $L = 12$ level. The second laser region excites about half of the population in the $L = 11$ level up to $n = 73$, where it is subsequently Stark ionized. This creates a current of Th^{4+} ions that can be charge selected and collected in a channel electron multiplier. If the frequency and amplitude of the rf electric field encountered between the laser regions is correct to drive a resonant transition between $L = 11$ and $L = 12$, this will change the population of $L = 11$ entering the second laser region and the eventual current of Th^{4+} ions collected after Stark ionization. To measure the transition, both lasers are left unchopped and the rf power is modulated at 2 kHz as a synchronous change in the Th^{4+} current is measured. Figure 2 illustrates one such resonance curve observed as the frequency of the rf electric field is varied. The width of the resonance, $\sim$2.4 MHz, is due to the transit time through the rf region and the unresolved splitting (1.03 MHz) between the two spin components of the transition. The Gaussian fit shown in Fig. 2 determined the center frequency to a precision of $\sim$0.1 MHz.

The rf interaction region used here was a shorter version of the eccentric coaxial transmission line used in Ref. [2]. The

---

[*]lundeen@lamar.colostate.edu
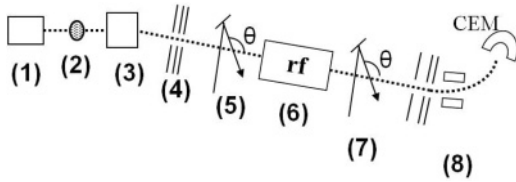
FIG. 1. Diagram of the microwave RESIS apparatus. A beam of the Th^{4+} is produced using an ECR and charge and mass selected at (1). The beam then passes through a dense Rb target at (2) where it charge captures a highly excited Rydberg electron to become a beam of Th^{3+} Rydberg states. The beams are then charge analyzed at (3) to select just the Th^{3+} Rydberg beam. An electrostatic lens then focuses that beam and ionizes any weakly bound Rydberg states, (4). At (5) a Doppler-tuned CO_2 laser excites transitions between a specific nL level to the higher n' level, depleting the population in the nL level. Then the rf region, if on resonance with a transitions, will repopulate the nL level at (6). A second Doppler-tuned CO_2 laser then excites the population of the nL level again the to the higher n' level at (7). The n' level is then Stark ionized and deflected into the channel electron multiplier at (8).

active length of the region, 12.7 cm, produced an interaction time of 0.44 μs for the 100-keV Th^{3+} ions. The diameters of the outer and inner conductors were 3.29 cm and 0.62 cm, respectively, and the eccentric offset was chosen to produce an impedance of 50 Ω [5]. The rf electric field propagated either parallel or antiparallel to the ion beam velocity, and data were taken in both directions and averaged to obtain the unshifted resonance position. Table I lists the transitions measured in this work. Four single-photon transitions were measured. Because $L = 12$ was the highest L level that could be reliably resolved in the RESIS excitation, levels above $L = 13$ were studied using two- and three-photon transitions [6]. At the higher rf powers needed for the multiphoton transitions, ac shifts of the resonance positions were significant. The shift rate of the three-photon 12–15 transition was directly measured, and the quoted result in Table I represents the linearly extrapolated result at zero power. The much smaller ac shift of the two-photon 12–14 transition was inferred from a calculation of the relative shift rates of the two- and three-photon transitions. The final column in Table I summarizes the measured fine-structure intervals.

In earlier studies, one concern was the possible buildup of stray electric fields within the rf interaction region that could Stark-shift the transition under study. As a check on
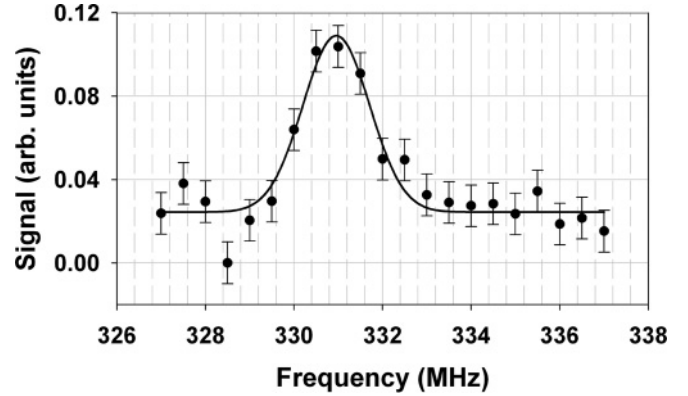
FIG. 2. The figure illustrates a RESIS rf signal representing the transition between the $L = 11$ and $L = 12$ levels of the $n = 37$ state of Th^{3+}. The rf electric field is propagating antiparallel to the ion beam velocity. Each data point represents 2 min of data taking. The width of the line is due to the transit time through the rf region and the unresolved spin splitting.

such effects in this study, the transition most sensitive to such shifts, the three-photon 12–15 transition, was measured repeatedly during the data collection period. Comparison of the observed resonance positions gave no evidence of variation in the possible stray field. Once the pattern of fine-structure intervals was measured, the presence of any stray field should be revealed, as in previous studies [2], by the effect of such a field on the pattern of fine-structure intervals. The Stark-shift rates of each interval are easily estimated once an approximate level pattern is known. Table II lists the calculated rates for each interval. In this case, a fit of the data pattern, including the effect of an arbitrary constant stray electric field, found a stray electric field amplitude consistent with zero with 0.01 V/cm precision. It thus appears that stray fields are not a significant factor in this measurement.

III. ANALYSIS

The fine-structure pattern in these high-L Rydberg levels is primarily determined by the expectation value of an effective potential whose first two terms are

$$V_{\text{eff}}(r) = -\frac{\alpha_D}{2}\frac{1}{r^4} - \frac{1}{2}(\alpha_Q - 6\beta_D)\frac{1}{r^6} + \cdots . \qquad (1)$$

TABLE I. Measured fine-structure intervals in $n = 37$ of Th^{3+}. Column 1 identifies the transitions, listing the two Ls whose separation is measured by their numerical value. Column 2 gives the standard identification using spectroscopy notation, although this becomes awkward for such high Ls. Column 3 shows the number of independent observations, column 4 shows the net correction due to ac shifts of the resonance position, and column 5 gives the measured interval.

Interval (L-L')		# No. of Observations	Δf_{ac}(MHz)	f_0(MHz)
9-10	M-N	2	0	1008.63(25)
10-11	N-O	6	0	562.08(10)
11-12	O-Q	6	0	331.34(6)
12-13	Q-R	5	0	204.60(13)
12-14	Q-T	5	−0.16(6)	335.78(12)
12-15	Q-U	4	−0.66(36)	423.15(39)

TABLE II. Corrections applied to infer the portion of the measured intervals due to the expectation value of V_{eff}. Column 1 lists the interval, column 2 shows the calculated relativistic contribution to the interval, column 3 shows the calculated second-order contribution of V_{eff}, including only the leading term, and column 4 shows the corrected interval. For reference, column 5 lists the dc Stark-shift rate of each interval.

Interval (L-L')	ΔE_{rel} (MHz)	$\Delta E^{[2]}$ (MHz)	$\Delta E^{[1]}$ (MHz)	κ (MHz/(V/cm)²)
9-10	8.88	1.90	997.85(25)	−20
10-11	7.33	0.59	554.16(10)	−28
11-12	6.16	0.20	324.98(6)	−38
12-13	5.25	0.08	199.27(13)	−49
12-14	9.77	0.11	325.90(12)	−109
12-15	13.71	0.12	409.32(39)	−183

The parameters α_{D} and α_{Q} are the adiabatic dipole and quadrupole polarizabilities and β_{D} is the first nonadiabatic dipole polarizability. The difference in the expectation values of V_{eff} in the two fine-structure levels contributes most of the measured interval, but two small additional contributions come from (a) relativistic corrections, and (b) the second-order effect of V_{eff}. The first is the standard first relativistic correction to the energy of a hydrogenic level. The second of these is calculated analytically in the approximation that only the first term in V_{eff} is significant in second order [7]. The full fine-structure interval is expected to be given by

$$E(n,L') - E(n,L) = \Delta E^{[1]} + \Delta E_{\mathrm{rel}} + \Delta E^{[2]}. \qquad (2)$$

In order to extract core properties from the measured intervals, the last two contributions were calculated and subtracted, leaving modified intervals due only to the expectation value of V_{eff}, which we denote as $\Delta E^{[1]}$. Table II shows these corrections and the inferred values of $\Delta E^{[1]}$.

If Eq. (1) gives the only significant terms in V_{eff}, then the intervals $\Delta E^{[1]}$ are expected to form a straight line when scaled and plotted as suggested in Eq. (3):

$$\frac{\Delta E^{[1]}}{\Delta \langle r^{-4} \rangle} = B_4 + B_6 \frac{\Delta \langle r^{-6} \rangle}{\Delta \langle r^{-4} \rangle}, \qquad (3)$$

where the fitted coefficients B_4 and B_6 would be identical to the coefficients in V_{eff}, C_4, and C_6. The radial expectation values needed to form this scaled plot are hydrogenic values, scaled to account for the mass of the Th⁴⁺ core ion. Figure 3 shows such a scaled plot with a linear fit to Eq. (3) represented by the dotted line. Quite obviously, the data are not consistent with a simple straight line. Instead, it clearly shows curvature, suggesting that additional terms in V_{eff}, proportional to higher inverse powers of r are contributing to the measured intervals. Many of these terms have been formally calculated, giving an extended potential of the form

$$V_{\mathrm{eff}}(r) = -\frac{\alpha_{\mathrm{D}}}{2}\frac{1}{r^4} - \frac{1}{2}(\alpha_{\mathrm{Q}} - 6\beta_{\mathrm{D}})\frac{1}{r^6} + \left(\frac{8Q}{5}\gamma_{\mathrm{D}} + \frac{\delta}{2}\right)\frac{1}{r^7}$$
$$- \frac{18}{5}\gamma_{\mathrm{D}}\frac{L(L+1)}{r^8} - C_8\frac{1}{r^8} + \cdots, \qquad (4)$$

where the coefficients occurring in V_{eff} are all properties of the Th⁴⁺ ion [8]. The parameter γ_{D} is the second nonadiabatic
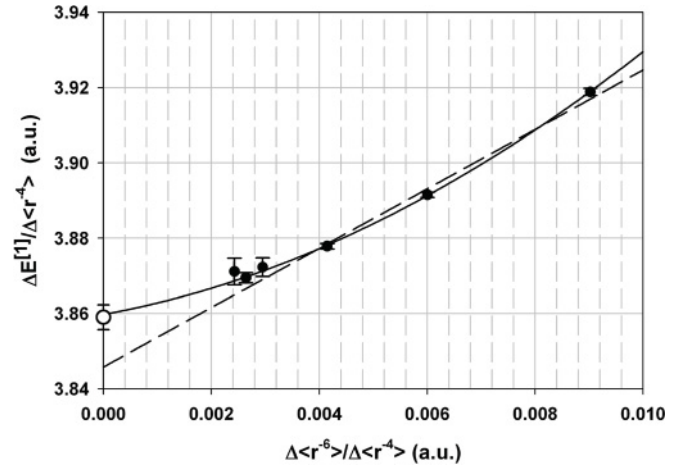
FIG. 3. Plot of the scaled first-order energies measured in this study. The data are the solid black points with error bar; on some points the error bar lies inside the point itself. The dotted line is the linear fit of the data that clearly fails to account for the measurements. The solid line is a fit that includes terms proportional to $\langle r^{-8} \rangle$, as described in the text. This second fit matches the data within the measurement precision and gives the y intercept shown by the open circle.

dipole polarizability, and the parameter δ determines the size of the first adiabatic contribution from the third-order perturbation energy. The parameter C_8 represents the net contribution of several higher-order terms. All of these parameters except C_8 are defined in terms of Th⁴⁺ matrix elements and excitation energies in the Appendix. For simplicity, we will refer to the total coefficient of the several powers of r according to

$$V_{\mathrm{eff}} = -\frac{C_4}{r^4} - \frac{C_6}{r^6} - \frac{C_7}{r^7} - C_{8L}\frac{L(L+1)}{r^8} - \frac{C_8}{r^8} + \cdots. \qquad (5)$$

Distinguishing the contributions of these various terms to fine-structure energies depends on the fact that the expectation values of the higher inverse powers decreases more rapidly with L than that of the lower inverse powers. For that reason, the contribution proportional to $L(L+1)r^{-8}$ is considered separately from the term proportional to r^{-8} since its behavior with L is similar to r^{-7}.

A previous study [8] concluded that it is impractical to extract the five C_i coefficients independently from a fit of data such as represented in Fig. 3. Instead, the data can be accurately parametrized by three parameters, B_4, B_6, and B_8 in the following function:

$$\frac{\Delta E^{[1]}}{\Delta \langle r^{-4} \rangle} = B_4 + B_6 \frac{\Delta \langle r^{-6} \rangle}{\Delta \langle r^{-4} \rangle} + B_8 \frac{\Delta \langle r^{-8} \rangle}{\Delta \langle r^{-4} \rangle}. \qquad (6)$$

The solid line in Fig. 3 shows a fit to Eq. (6), an excellent fit to all the data. The fitted parameters are

$$B_4 = 3.8590(33), \quad B_6 = 3.0(1.5), \quad B_8 = 391(91).$$

If the contribution of the term in V_{eff} proportional to C_7 and C_{8L} are not significant, then the fitted parameters B_4 and B_6 can be identified as the coefficients C_4 and C_6. If, however, the C_7 and C_{8L} contributions are not negligible this can alter that interpretation. Fortunately, the possible contributions of

these additional terms can also be parametrized by Eq. (6). Scaling their contributions for unit coefficients in the same way as the data, and fitting to Eq. (6) using the same relative weights as were used for the experimental measurements, an excellent-quality fit was obtained in each case with the results;

$$\frac{\Delta\langle r^{-7}\rangle}{\Delta\langle r^{-4}\rangle} \rightarrow \ B_4 = -4.7(5) \times 10^{-5},$$

$$B_6 = 0.0555(18), \quad B_8 = 4.86(15),$$

$$\frac{\Delta[L(L+1)\langle r^{-8}\rangle]}{\Delta\langle r^{-4}\rangle} \rightarrow \ B_4 = -3.5(4) \times 10^{-4},$$

$$B_6 = 0.397(13), \quad B_8 = 44.4(1.1),$$

where the uncertainties attached to the fitted coefficients reflect the precision of the fits.

Based on these fits, it can be seen that nonzero values of C_7 and C_{8L} would affect the fitted values of both B_4 and B_6 according to

$$B_4 = C_4 - [4.7(5) \times 10^{-5}]\,C_7 - [3.5(4)10^{-4}]\,C_{8L}$$
(7)
$$B_6 = C_6 + [0.056(2)]\,C_7 + [0.40(1)]\,C_{8L}.$$

Rewriting Eq. (7) in term of core properties,

$$B_4 = \frac{\alpha_D}{2} - [1.0(1) \times 10^{-3}]\gamma_D + [2.4(3)10^{-5}]\delta,$$
(8)
$$B_6 = \frac{\alpha_Q}{2} - 3\beta_D + [1.07(5)]\gamma_D - [0.028(1)]\delta.$$

Clearly, if both γ_D and δ are zero, the simplest interpretation of the fit parameters in terms of core properties is valid, but

if γ_D or δ is sufficiently large, that interpretation may be significantly in error. Since the dependence of B_4 on these parameters is very slight, the most significant effect is likely to be in the parameter B_6.

In order to determine the size of the final two terms in Eq. (8), it is necessary to estimate the core properties γ_D and δ. This is relatively easy in the case of γ_D as it is related to the same set of matrix elements and excitation energies that determine α_D and β_D:

$$\alpha_D \equiv \frac{2}{3}\sum_{\lambda'}\frac{\langle gJ=0\|\vec{D}\|\lambda'J=1\rangle^2}{\Delta E(\lambda')},$$

$$\beta_D \equiv \frac{1}{3}\sum_{\lambda'}\frac{\langle gJ=0\|\vec{D}\|\lambda'J=1\rangle^2}{\Delta E(\lambda')^2},$$
(9)
$$\gamma_D \equiv \frac{1}{6}\sum_{\lambda'}\frac{\langle gJ=0\|\vec{D}\|\lambda'J=1\rangle^2}{\Delta E(\lambda')^3}.$$

Theoretical calculations [9,10] of the first two parameters, $\alpha_D = 7.75$ a.u. and $\beta_D = 2.97$ a.u., suggest that the average excitation energy of the contributing states is 1.3 a.u, and therefore that $\gamma_D \approx 1.1$ a.u. This value, which is probably good to 10% makes its contribution to B_4 smaller than the experimental error in this study. Its contribution to B_6, however, is significant.

Obtaining an estimate of the parameter δ is much more difficult. As the definition shows, δ is related to dipole and quadrupole matrix elements between core and excited levels, and the excitation energies of these levels:

$$\delta \equiv \frac{4\sqrt{2}}{15}\sum_{\lambda',\lambda''}\frac{\langle gJ=0\|\vec{D}\|\lambda'J=1\rangle\langle\lambda'J=1\|\vec{D}\|\lambda''J=2\rangle\langle\lambda''J=2\|\overset{\leftrightarrow}{Q}\|gJ=0\rangle}{\Delta E(\lambda')\Delta E(\lambda'')}$$

$$+\frac{2\sqrt{30}}{45}\sum_{\lambda',\lambda''}\frac{\langle gJ=0\|\vec{D}\|\lambda'J=1\rangle\langle\lambda'J=1\|\overset{\leftrightarrow}{Q}\|\lambda''J=1\rangle\langle\lambda''J=1|\vec{D}\|gJ=0\rangle}{\Delta E(\lambda')\Delta E(\lambda'')}.$$
(10)

In view of the complete absence of experimental information about the position of such levels, this is a challenging undertaking. Fortunately, all the excited levels of Th^{4+} are expected to be rather high in energy, making the denominators of Eq. (10) relatively large. Estimates of the level energies in the $6p^55f$, $6p^56d$, and $6p^57s$ configurations, obtained in the Dirac Hartree Fock (DHF) approximation, and order-of-magnitude estimates of the relevant dipole and quadrupole matrix elements [11] suggest that the magnitude of δ does not exceed 30 a.u. This would indicate that the contribution of δ to B_4 is negligible at the level of experimental precision in this study, but again the contribution to B_6 could be significant. Since the sign of δ is not necessarily positive or negative, we assign a value,

$$\delta = 0 \pm 30 \ \text{a.u.}$$

From Eq. (8), the fitted coefficient B_4 gives a determination of α_D, the dipole polarizability of Th^{4+}. In this case the contributions from γ_D and δ are very small:

$$\alpha_d = 2B_4 + 0.0020(2)\gamma_D = 7.720(7).$$

This result improves upon the precision of the result obtained from the optical data [1] by approximately one order of magnitude. Both values are shown in Table III, along with several theoretical calculations. Agreement to better than 0.5% is found both with a recent relativistic coupled-cluster [RCCSD(T)] calculation [12], and with a relativistic random phase approximation (RRPA) calculation [9]. A fully relativistic Dirac Hartree Fock calculation is in error by 16% and a nonrelativistic Hartree Fock calculation misses by 33%.

TABLE III. Comparison of measured and calculated polarizabilities of Th^{4+}. All results are in atomic units. The experimental results for α_Q rely on calculated values of β_D, γ_D, and δ, as described in the text.

	α_D (a.u.)	α_Q (a.u.)
Experiment	7.720(7)[a]	21.5(3.9)[a]
	7.61(6)[b]	47(11)[b]
Theory	7.699[c]	
	7.75[d]	28.8[e]
	8.96[f]	24.5[f]
	10.26[g]	

[a]This work.
[b]Reference [1].
[c]RCCSD(T), Schwerdtfeger and Borschevsky [12].
[d]RRPA, Safronova *et al.* [9].
[e]RRPA, Safronova [10].
[f]DHF, Safronova [10].
[g]Fraga, Karwowski, and Saxena [13].

The fitted value of B_6 determines α_Q, the quadrupole polarizability of Th^{4+}, according to Eq. (8). Using calculated estimates of β_D ($\beta_D = 2.97$ a.u. [10]), the simple estimate of γ_D discussed previously ($\gamma_D = 1.1$), and the primitive estimate of δ ($\delta = 0 \pm 30$ a.u.), α_Q is determined to be

$$\begin{aligned} \alpha_Q &= 2B_6 + 6\beta_D - 2.14\gamma_D + 0.056\delta, \\ &= 6.0(3.0) + 17.8(1.8) - 2.3(2) + 0(1.7) = 21.5(3.9). \end{aligned}$$

Clearly, this is not a purely experimental result, as it depends on calculation of the three parameters β_D, γ_D, and δ, but knowledge of these calculated properties is not the limiting factor in the measurement as the precision is largely due to the uncertainty in B_6. In this current study a 10% uncertainty of β_D and γ_D was assumed. This is likely an overestimate of their uncertainty. The RRPA calculation completed of β_D used the same method that calculated α_d and agreed with our measurement to better than 1%.

Both the present and the previous experimental values for α_Q are shown in Table III. The current measurement differs significantly from the result reported previously in the optical RESIS study [1]. The primary reason for the difference is that the optical data were parametrized by a linear fit. This was sufficient to account for the less precise optical data, but it gave a much larger value of B_6 [13(2)]. Analysis of the optical data also neglected the contributions of γ_D and δ, but this had much less effect on the inferred value of α_Q. The value of α_Q reported here is in fair agreement with calculations shown in Table III, although the agreement is not improved going from the uncorrelated Dirac Hartree Fock (DHF) to the presumably more accurate relativistic random

phase approximation (RRPA) calculation. The 18% precision of the present result for α_Q could be improved if the precise rf data pattern could be extended to lower L states to more precisely define the curvature of the polarization plot, or if the individual fine-structure intervals could be measured with higher precision. It would also be helpful to have actual calculations of the parameters γ_D and δ to replace the estimates made here.

IV. CONCLUSIONS

The dipole and quadrupole polarizabilities of Rn-like Th^{4+} have been measured through spectroscopy of high-L Rydberg levels of Th^{3+}. The new value of α_D is an order of magnitude more precise than the previous measurement [1]. The new value of α_Q differs significantly from a previous report due to the influence of higher-order terms in the effective potential describing the interaction between Rydberg electron and Th^{4+} core. Both measured polarizabilities represent demanding tests of *a priori* theoretical methods used to describe the Rn-like Th^{4+} ion.

APPENDIX

The core properties that appear in the full effective potential in the text are explicitly defined in term of matrix elements and excitation energies of the free Th^{4+} ion:

$$\alpha_D \equiv \frac{2}{3} \sum_{\lambda'} \frac{\langle gJ = 0 \| \vec{D} \| \lambda' J = 1 \rangle^2}{\Delta E(\lambda')},$$

$$\alpha_Q \equiv \frac{2}{5} \sum_{\lambda'} \frac{\langle gJ = 0 \| \overleftrightarrow{Q} \| \lambda' J = 2 \rangle^2}{\Delta E(\lambda')},$$

$$\beta_D \equiv \frac{1}{3} \sum_{\lambda'} \frac{\langle gJ = 0 \| \vec{D} \| \lambda' J = 1 \rangle^2}{\Delta E(\lambda')^2},$$

$$\gamma_D \equiv \frac{1}{6} \sum_{\lambda'} \frac{\langle gJ = 0 \| \vec{D} \| \lambda' J = 1 \rangle^2}{\Delta E(\lambda')^3},$$

$$\begin{aligned} \delta \equiv{}& \frac{4\sqrt{2}}{15} \sum_{\lambda',\lambda''} \frac{\langle gJ = 0 \| \vec{D} \| \lambda' J = 1 \rangle \langle \lambda' J = 1 \| \vec{D} \| \lambda'' J = 2 \rangle \langle \lambda'' J = 2 \| \overleftrightarrow{Q} \| gJ = 0 \rangle}{\Delta E(\lambda') \Delta E(\lambda'')}, \\ &+ \frac{2\sqrt{30}}{45} \sum_{\lambda',\lambda''} \frac{\langle gJ = 0 \| \vec{D} \| \lambda' J = 1 \rangle \langle \lambda' J = 1 \| \overleftrightarrow{Q} \| \lambda'' J = 1 \rangle \langle \lambda'' J = 1 \| \vec{D} \| gJ = 0 \rangle}{\Delta E(\lambda') \Delta E(\lambda'')}. \end{aligned}$$

J denotes the angular momentum of the state and the sum over all possible excited states. The dipole and quadrupole operators aredefined by

$$\vec{D} \equiv \sum_{i=1}^{86} r_i C^{[1]}(\hat{r}_i), \qquad \overset{\leftrightarrow}{Q} \equiv \sum_{i=1}^{86} r_i^2 C^{[2]}(\hat{r}_i).$$

[1] M. E. Hanni, J. A. Keele, S. R. Lundeen, and C. W. Fehrenbach, Phys. Rev. A **82**, 022512 (2010).

[2] R. A. Komara, M. A. Gearba, S. R. Lundeen, and C. W. Fehrenbach, Phys. Rev. A **67**, 062502 (2003).

[3] M. E. Hanni, J. A. Keele, S. R. Lundeen, C. W. Fehrenbach, and W. G. Sturrus, Phys. Rev. A **81**, 042512 (2010).

[4] D. S. Fisher, S. R. Lundeen, C. W. Fehrenbach, and B. D. DePaola, Phys. Rev. A **63**, 052712 (2001).

[5] *Reference Data for Engineers: Radio, Electronics, Computer and Communications*, 8th ed., edited by M. E. Van Valkenburg (SAMS, Indianapolis, 1995).

[6] J. R. Brandenberger, S. R. Lundeen, and F. M. Pipkin, Phys. Rev. A **14**, 341 (1976).

[7] G. W. F. Drake and R. A. Swainson, Phys. Rev. A **44**, 5448 (1991).

[8] E. L. Snow and S. R. Lundeen, Phys. Rev. A **75**, 062512 (2007).

[9] U. I. Safronova, W. R. Johnson, and M. S. Safronova, Phys. Rev. A **74**, 042511 (2006).

[10] M. S. Safronova (private communication).

[11] D. R. Beck (private communication).

[12] P. Schwerdtfeger and A. Borschevsky (private communication).

[13] S. Fraga, J. Karwowski, and K. M. Saxena, *Handbook of Atomic Data* (Elsevier, Amsterdam, 1976).